Structure of ice IV, a metastable highpressure phase

Hermann Engelhardt and Barclay Kamb

Citation: The Journal of Chemical Physics **75**, 5887 (1981); doi: 10.1063/1.442040
View online: http://dx.doi.org/10.1063/1.442040
View Table of Contents: http://scitation.aip.org/content/aip/journal/jcp/75/12?ver=pdfcov
Published by the AIP Publishing

Structure of ice IV, a metastable high-pressure phase

Hermann Engelhardt and Barclay Kamb

Division of Geological and Planetary Sciences,[a] California Institute of Technology, Pasadena, California 91125
(Received 8 June 1979; accepted 31 August 1981)

Ice IV, made metastably at pressures of about 4 to 5.5 kb, has a structure based on a rhombohedral unit cell of dimensions $a_R = 760 \pm 1$ pm, $\alpha = 70.1 \pm 0.2°$, space group $R\bar{3}c$, as observed by x-ray diffraction at 1 atm, 110 K. The cell contains 12 water molecules of type 1, in general position, plus 4 of type 2, with O(2) in a special position on the threefold axis. The calculated density at 1 atm, 110 K is 1.272 ± 0.005 g cm^{-3}. Every molecule is linked by asymmetric H bonds to four others, the bonds forming a new type of tetrahedrally-connected network. Molecules of type 1 are linked by O(1)···O(1′) bonds into puckered six-rings of $\bar{3}$ symmetry, through the center of each of which passes an O(2)···O(2′) bond between a pair of type-2 molecules, along the threefold axis. The six-rings are linked laterally by type-2 molecules to form puckered sheets that are topologically similar to such sheets in ice I, but are connected to one another in a very different and novel way. One quarter of the intersheet bonds connect not directly between adjacent sheets but remotely, from one sheet to the second nearest sheet, through holes in the intervening sheet. These remote connections are the O(2)···O(2′) bonds, passing through the O(1)-type six-rings. The sheets are stacked in a sequence based on ice Ic, modified by reversal of the puckering to form the remote connections and by internal distortion of the sheets to complete the remaining intersheet bonds. Of the four nonequivalent H bonded O···O distance in the structure, two (279 and 281 ± 1pm) are only moderately lengthened relative to the bonds in ice I (275 pm), whereas the O(1)···O(1′) bond (288 ± 1pm) and O(2)···O(2′) bond (292 ± 1pm) are lengthened extraordinarily. This is caused by repulsion between O(1) and O(2) at nonbonded distances of 314 and 329 pm in the molecular cluster consisting of the O(1)-type six-ring threaded by the O(2)···O(2′) bond. The mean O···O bond distance of 283.3 pm, which is high relative to other ice structures except ice VII/VIII, reflects similarly the accommodation of a relatively large number (3.75 on average) of nonbonded neighbors around each molecule at relatively short distances of 310–330 pm. Bond bending in ice IV, as measured by deviation of the O···O···O bond angles from 109.5°, is relatively low compared to most other dense ice structures. All H bonds in ice IV except O(1)···O(1′) are required to be proton-disordered by constraints of space-group symmetry. The x-ray structure-factor data indicate that O(1)···O(1′) is probably also proton-disordered. Ice IV is the only ice phase other than ice I and Ic to remain proton-disordered on quenching to 77 K. The increased internal energy of ice IV relative to ice V, amounting to about 0.23 kJ mol^{-1}, which underlies the metastability of ice IV in relation to ice V, can be explained structurally as a result of extra overlap and bond-stretching energy in ice IV, partially compensated by extra bond-bending energy in ice V. The structural relation between ice IV and ice I offers a possible explanation for the reduced barrier to nucleation of ice IV, as compared to ice V, in crystallizing from liquid water.

I. INTRODUCTION

Ice IV is a high-pressure phase that has no field of outright stability but can form metastably within the stability field of ice V. It was discovered by Bridgman,[1] and its existence was verified[2,3] in experiments showing that its melting-point curve, as a function of pressure, is definitely distinguishable from the melting curves of ices III, V, and VI. Further physical characterization was made possible by successful quenching of samples of ice IV to liquid nitrogen temperature and extraction to atmospheric pressure.[3] Infrared spectroscopic data from such samples have been reported.[4] We here report x-ray data and the results of an x-ray structure determination, which provide the most detailed characterization of ice IV thus far achieved.[5] The results are of interest in relation to questions of molecular rearrangement in hydrogen-bonded solids under pressure, hydrogen-bond distortion, proton order/disorder, and the structural basis for metastable crystallization. They augment existing structural information on ice polymorphism and its relation to the bonding characteristics of the water molecule.[6,7]

II. EXPERIMENTAL METHODS

The ice IV used in this investigation was made by Engelhardt and Whalley[3] in the Division of Chemistry of the National Research Council of Canada, Ottawa, and preserved there in liquid nitrogen. We used material from sample S. 119, made from D_2O with a small amount of powdered tetrachloro-phthalic anhydride (TCPA) added as nucleating agent. The ice, immersed in liquid nitrogen, was broken into mm-size fragments which were loaded individually into Lindemann glass capillaries and then mounted and examined on a precession camera equipped to maintain the ice at 110 K in a stream of cold nitrogen gas.[8] Ten fragments were examined in this way, and of these, two were single crystals suitable for detailed crystallographic study. Crystal no. 1 was lost due to malfunction of the low-temperature apparatus, and most of the x-ray data were obtained from crystal no. 2. Rotation photographs made on the precession camera showed that all ten fragments gave the same x-ray powder pattern, which was identical to one obtained earlier from the same sample by L. D. Calvert. No powder lines from TCPA were detected.

III. X-RAY DATA

X-ray powder diffraction data for ice IV are given in Table I, to provide a primary characterization of the

[a]Contribution No. 3272. This paper is also contribution N.R.C. 19653 from the National Research Council of Canada.

 0021-9606/81/245887-13$01.00

TABLE I. X-ray powder diffraction data for ice IV at 1 atm, 110 K.

I_0	d_0[a] (pm)	d_c (pm)	$F_c^2\times10^{-4}m$[b]	$h\ k\ l$
m	572	566	8	0 1 1
vw	373	371	4	1 1 2
vw	342	346	7	0 1 2
		345	3	0 0 2
s	284	284	35	2 2 2
		283	121	0 2 2
s	282	282	107	0 2 $\bar{1}$
s	270	271	107	1 2 $\bar{1}$
m	251	252	35	1 1 $\bar{2}$
s	239	238	161	1 2 3
s	218	219	54	0 2 3
		218	66	0 2 $\bar{2}$
m	208	208	51	1 2 $\bar{2}$
		205	5	2 3 3
		189	16	1 1 4
m	185	185	32	1 2 4
m	178	179	66	0 1 4
		174	10	2 3 4
		173	17	0 0 4
		166	15	3 3 4
		165	14	1 2 $\bar{3}$
m	159	161	37	1 4 $\bar{1}$
		159	40	2 3 $\bar{2}$
		159	17	0 4 $\bar{1}$
		159	9	0 3 4
		155	15	2 4 4
s	142	146	25	2 3 5
		143	30	3 4 $\bar{1}$
		142	22	4 4 4
		141	24	0 4 $\bar{2}$
		141	9	0 4 4
w	133	136	12	2 4 5
		135	16	0 3 5
		135	15	1 2 $\bar{4}$
		134	27	2 3 $\bar{3}$
		132	20	1 4 5
		130	37	2 5 $\bar{1}$
m	125	126	14	3 4 $\bar{2}$
		125	32	2 3 6
		124	15	0 4 $\bar{3}$
		124	12	2 5 5
		124	24	0 4 5
w	119	121	35	1 3 $\bar{4}$
		119	24	2 4 6
		119	13	2 4 $\bar{3}$
		119	10	0 1 6
		118	11	0 5 $\bar{2}$
		115	19	0 0 6

[a]The uncertainty $\sigma(d_0)$ in d_0 due to measurement accuracy is estimated to be $\sigma(d_0)/d_0 = 2\times10^{-3}(d_0/\lambda)(1-\lambda^2/4d_0^2)^{1.5}$, where $\lambda = 71$ pm. Representative pairs of values (d_0, σ) are (570, 9), (280, 2), (180, 1), and (130, 0.3).

[b]m is the reflection multiplicity relative to that for the general $h\ k\ l$ reflection taken as unity. F_c is from Table II. d_c is calculated for a rhombohedral cell with $a_R = 760$ pm, $\alpha_R = 70.1°$.

phase. The observed intensities I_0 and lattice spacings d_0 were obtained from a flat film taken with Zr-filtered Mo $K\alpha$ radiation by rotation of a polycrystalline sample with precession angle 0.

The unit cell of ice IV, determined from precession photographs with Zr-filtered Mo $K\alpha$ radiation of assumed wavelength 71.0 69 pm, is rhombohedral, with cell size (at 1 atm, 110 K) $a_R = 760 \pm 1$ pm, $\alpha_R = 70.1 \pm 0.2°$. The corresponding hexagonal unit cell with volume three times the rhombohedral cell volume has dimensions $a_H = 874 \pm 1$ pm, $c_H = 1705 \pm 3$ pm. Table I shows that this cell and the single-crystal diffraction intensities account satisfactorily for the x-ray powder data.

Laue symmetry $\bar{3}m$ was revealed by precession photographs from crystal no. 1, for which the three-fold axis was directly observed. Photographs from crystal no. 2 were compatible with this. The Laue symmetry, cell geometry, and systematic extinctions hhl for l odd define the space group uniquely as $R\bar{3}c$.

Three-dimensional diffracted intensity data were collected with Zr-filtered Mo $K\alpha$ radiation in 26 precession photographs of nine reciprocal lattice planes[9] with various exposure times. About 2600 individual intensity values were read visually and corrected for Lorentz and polarization factors in the usual way,[10] without absorption correction. The corrected intensities I from different films were scaled together through common reflections by a least-squares procedure,[11a] and I values of equivalent reflections were then averaged and converted by standard procedures to observed structure factors F_0 on a preliminary, and later, a refined absolute scale. The latter values are listed in Table II, which contains all 206 reflections out to $d^* = 11.5$ nm^{-1} plus 70 reflections constituting an incomplete sampling of the range $d^* = 11.5$ to 14.3 nm^{-1}. Of the 276 reflections, measurable intensities were detected for 213; the remainder had intensities below an estimated limit $I_{\min}$. For the least-squares structure refinement, a weight w was assigned to each reflection by the formula[11b]

$$w = w_e[\tfrac{1}{3}I_{\min} + 0.05I + 0.1I^2/(I_{\max} - I)^2]^{-2},$$

where $I_{\max}$ is the upper limit of intensity that can be read from the photographic films. Here w_e is an "external weight" chosen as 1.0, 0.5, or 0 on the basis of a qualitative judgement as to the reliability of the intensity value. w was taken to be 0 for reflections weaker than the detection limit and for very strong reflections; an asterisk in Table II indicates $w = 0$, there being 87 such reflections.

IV. STRUCTURE DETERMINATION

The rhombohedral unit cell of ice IV contains 16 water molecules, as determined in the following way. Bridgman's[1] volumetric measurements on D_2O ice IV at 5.4 kb, $-6°$C correspond to a density of 1.38 g cm^{-3} at 1 atm, $-175°$C if the proportional change in density between the two P, T conditions is the same as for ice V, as estimated by Kamb *et al.*[12] This density corresponds to a cell content of 15.6 water molecules. Space group $R\bar{3}c$ requires that the cell content be an even number of molecules, so that 16 is indicated. The density calculated on this basis for H_2O ice IV at 1 atm, 110 K, under the assumption that the H_2O and D_2O ices have the same dimensions, is 1.272 ± 0.005 g cm^{-3}. This corresponds, by reversal of the procedure used above, to a

TABLE II. Observed (F_0) and calculated (F_c)[b] structure factors for ice IV.

h	k	l	F_0	F_c	h	k	l	F_0	F_c	h	k	l	F_0	F_c	h	k	l	F_0	F_c	h	k	l	F_0	F_c
0	0	2	230	260	0	6	−1*	86	78	1	5	−5*	83	62	2	5	−2	162	184	3	7	−3	55	59
0	0	4	640	587	0	6	6	288	316	1	5	−4	116	122	2	5	−1	620	606	3	7	8	254	280
0	0	6	643	620	0	6	7	163	136	1	5	−2	204	196	2	5	5	485	495	3	7	9	48	27
0	0	8	328	299	0	6	8	246	218	1	5	−1	69	86	2	5	6*	83	25	3	8	−1*	53	21
0	1	1*[a]	459	406	0	7	−4	188	137	1	5	6	71	51	2	5	7*	65	46	4	4	−4	399	364
0	1	2	240	264	0	7	−3*	68	62	1	5	7*	67	39	2	5	8	204	181	4	4	−2	267	257
0	1	3	211	207	0	7	−2	86	62	1	5	8	152	149	2	5	9	200	199	4	4	4*	1151	1158
0	1	4*	928	814	0	7	−1	109	131	1	6	−5	97	67	2	6	−5	251	199	4	4	6	279	267
0	1	5	265	257	0	8	−4	164	142	1	6	−3	88	121	2	6	−4*	47	38	4	4	8	236	221
0	1	6	283	311	0	8	−2	354	316	1	6	−2*	26	33	2	6	−3	157	159	4	5	−4*	85	17
0	1	7	237	222	0	8	−1*	45	29	1	6	−1*	61	41	2	6	−2	361	364	4	5	−3	277	279
0	1	8*	74	30	1	1	−6	213	220	1	6	7	155	166	2	6	−1	380	400	4	5	−2	129	123
0	2	−2*	1156	1172	1	1	−4	115	119	1	6	8	134	123	2	6	6*	65	69	4	5	−1	86	117
0	2	−1*	979	1034	1	1	−2*	799	830	1	7	−4	159	185	2	6	7	328	299	4	5	5	102	93
0	2	2*	1447	1556	1	1	2	255	274	1	7	−3*	57	60	2	6	8	49	53	4	5	6	260	262
0	2	3	741	737	1	1	4	594	562	1	7	−2	58	76	2	6	9	82	84	4	5	7*	74	49
0	2	4*	69	6	1	1	6*	62	33	1	7	−1*	67	32	2	7	−4*	81	31	4	5	8	340	326
0	2	5	199	209	1	1	8	71	49	1	8	−3*	150	62	2	7	−2	319	303	4	6	−4	154	156
0	2	6	107	95	1	2	−7	77	79	1	8	−2	179	152	2	7	−1	163	168	4	6	−3	90	92
0	2	7	216	224	1	2	−6*	87	47	1	8	−1	187	173	2	7	7	272	287	4	6	−2	411	381
0	2	8	137	142	1	2	−5	98	79	2	2	−6	573	553	2	7	8	98	101	4	6	−1	227	239
0	2	9	117	106	1	2	−4	413	388	2	2	−4*	69	42	2	7	9*	94	38	4	6	6	663	616
0	3	−3*	66	36	1	2	−3	428	377	2	2	−2	220	209	2	8	−1	186	167	4	6	7	139	122
0	3	−2*	47	54	1	2	−2*	680	713	2	2	2*	1409	1447	2	9	−1	164	167	4	6	8	79	77
0	3	−1	223	232	1	2	−1*	988	1035	2	2	4	139	185	3	3	−4	96	77	4	6	9	146	157
0	3	3	274	284	1	2	3*	1284	1267	2	2	6	67	58	3	3	−2	332	335	4	7	−3*	70	73
0	3	4	303	299	1	2	4*	642	565	2	2	8	157	160	3	3	4	565	542	4	7	−2	156	172
0	3	5	374	394	1	2	5	304	289	2	3	−6*	104	24	3	3	6	163	160	4	7	−1	180	191
0	3	6	192	175	1	2	6	90	89	2	3	−5	171	177	3	3	8	186	167	4	7	7*	55	9
0	3	7*	70	15	1	2	7	341	319	2	3	−4*	87	24	3	4	−5	129	134	4	7	8	107	82
0	3	8	56	42	1	2	8	108	133	2	3	−3	519	518	3	4	−4*	88	54	4	7	9	61	50
0	3	9	200	168	1	3	−7*	84	37	2	3	−2	679	629	3	4	−3	302	304	4	8	8	87	72
0	3	10*	145	91	1	3	−6*	68	66	2	3	−1*	61	26	3	4	−2	368	373	5	5	−2*	69	62
0	4	−4*	81	55	1	3	−5*	65	42	2	3	3	391	319	3	4	−1	532	552	5	5	6*	86	39
0	4	−3	373	387	1	3	−4	650	594	2	3	4	346	323	3	4	5*	64	23	5	5	8	243	267
0	4	−2	520	485	1	3	−3	70	79	2	3	5	528	499	3	4	6	239	240	5	6	−2*	78	32
0	4	−1	401	410	1	3	−2	175	169	2	3	6	640	567	3	4	7	74	71	5	6	−1*	92	12
0	4	4	418	425	1	3	−1*	48	41	2	3	7	347	337	3	4	8*	76	64	5	6	7	250	269
0	4	5	499	493	1	3	4	142	176	2	3	8	121	155	3	4	9*	62	9	5	6	8	78	72
0	4	6	288	296	1	3	5	59	32	2	3	9*	53	22	3	5	−5*	89	40	5	7	−3*	52	37
0	4	7*	69	0	1	3	6	57	50	2	4	−6*	64	16	3	5	−4	217	229	5	7	−2*	62	18
0	4	8*	48	61	1	3	7	62	59	2	4	−5*	68	9	3	5	−3*	66	38	5	7	−1*	68	35
0	4	9	246	245	1	3	8	326	331	2	4	−4	159	148	3	5	−2*	58	23	5	7	8*	52	10
0	5	−5	51	36	1	3	9*	63	22	2	4	−3	328	355	3	5	−1*	57	40	5	7	9*	50	12
0	5	−4	270	273	1	4	−6	215	184	2	4	−2	118	112	3	5	6	192	194	5	8	−2	86	92
0	5	−3	77	67	1	4	−5	295	296	2	4	−1	164	192	3	5	7*	69	13	5	8	−1*	283	183
0	5	−2	351	338	1	4	−4	54	50	2	4	4	533	538	3	5	8	207	216	6	6	6	72	82
0	5	−1	134	144	1	4	−3	153	164	2	4	5	372	342	3	5	9	51	48	6	6	8	204	168
0	5	5*	86	34	1	4	−2	56	53	2	4	6	453	487	3	5	10*	99	40	6	6	10*	66	64
0	5	6	234	226	1	4	−1	718	609	2	4	7	188	209	3	6	−4	193	155	6	7	7	150	162
0	5	7	354	340	1	4	5	431	445	2	4	8	156	162	3	6	−3	52	65	6	7	8	134	180
0	5	8*	42	47	1	4	6	186	202	2	4	9	103	101	3	6	−2	58	68	6	7	9	115	105
0	6	−5*	47	31	1	4	7*	44	34	2	4	10*	61	32	3	6	−1*	56	1	6	8	8	155	167
0	6	−4	225	213	1	4	8	286	297	2	5	−5	236	228	3	6	7*	85	49	6	9	−1	89	110
0	6	−3	237	230	1	4	9*	49	59	2	5	−4	229	244	3	6	8	161	176	7	7	8	274	217
0	6	−2	208	214	1	5	−6	188	149	2	5	−3	63	66	3	7	−4*	154	134					

[a]The asterisk indicates zero weight in structure refinement (see text). For unobserved reflections, the F_0 value given is the detection limit.

[b]The F_c values given are calculated for half-hydrogens in positions on oxygen–oxygen center lines (Table IV) and for O(1) at position (0.3798, −0.1108, −0.2397) and O(2) at (0.0856, 0.0856, 0.0856), which differ slightly from the final refined positions (Table III). h, k, l are rhombohedral indices.

calculated density 1.320 g cm^{-3} for H_2O ice IV at 5.4 kb, −6 °C. The density based on x-ray measurements is thus, 2% higher than the value 1.29 g cm^{-3} based on Bridgman's volumetric measurements,[1] a situation similar to that found for ices V, VI, and VII.[12]

Of the available positions for the oxygen atoms in space group $R3\bar{c}$, positions of types 2*a*, 2*b*, and 6*d* are ruled out because they lie at lattice points of $\bar{3}$, 32, and $\bar{1}$ symmetry, respectively, which are unsuitable if the water molecules are in tetrahedral coordination as in

TABLE III. Position coordinates[a] and thermal-motion parameters[b] for oxygen atoms in the ice IV structure.

Atom type	O(1)	O(2)
Position type	12*f*	4*c*
x	0.3804	0.0855
y	−0.1109	0.0855
z	−0.2396	0.0855
β_{11}	103	75
β_{22}	73	75
β_{33}	94	75
β_{12}	−21	−42
β_{13}	−39	−42
β_{23}	−92	−42

[a]Atomic coordinates are dimensionless fractions of the rhombohedral axial length. Estimated standard deviation is 0.0005 (see text).

[b]The Debye-Waller factor is $\exp(-\beta_{11}h^2 - \beta_{22}k^2 - \beta_{33}l^2 - \beta_{12}hk - \beta_{23}kl - \beta_{13}hl)$. The values given for β_{ij} in the table have been multiplied by 10^4. Estimated standard deviation is about four in the last decimal place given.

other known ice structures. Not all of the oxygen atoms can be in positions of type 4*c*, because they would have to lie much too close together (106 pm or less). Trial and error consideration of the remaining possibilities, with the help of the three-dimensional Patterson function calculated from the data in Table II, led to a structure involving a set of 12 oxygen atoms [called O(1)] in general position 12*f* and a set of four [called O(2)] in special position 4*c*, on the three-fold axes. This arrangement gave an initial residual $R = \Sigma||F_0| - |F_c||/\Sigma|F_0| = 0.44$ for the average discrepancy between observed and calculated structure factors.

V. STRUCTURE REFINEMENT

Least-squares refinement of oxygen coordinates and anisotropic temperature parameters, with omission of hydrogen atoms, converged to $R = 0.078$. The function minimized in the refinement is $\Sigma w^2 (F_0^2 - F_c^2)^2$, summed over the reflections in Table II. Standard scattering factors[13] were used in calculating F_c.[14]

Because symmetry and bonding relations suggest hydrogen disorder analogous to that in ice I (see Sec. VIII), hydrogen-atom positions with occupancy factor $\frac{1}{2}$ and assumed isotropic thermal-motion parameter $B = 1.9 \times 10^4$ pm^2 were introduced at points on the nearest-neighbor oxygen–oxygen center lines 98 pm from the oxygen atoms at each end. Without further refinement, R improved to 0.068. Oxygen parameters were then refined again, keeping the hydrogen fixed. Final coordinate shifts were less than 0.0005, with estimated standard deviations between 0.0002 and 0.0005, and R remained 0.068. Hydrogen coordinates were then refined, leading to $R = 0.067$. The final parameters, at the end of this refinement procedure, are listed in Tables III and IV, and calculated structure factors F_c are given in Table II. The final weighted residual $R_w = \Sigma w^2 (F_0^2 - F_c^2)^2 / \Sigma w^2 F_0^4$ is 0.02.

VI. DESCRIPTION OF THE STRUCTURE

The structure of ice IV is shown in Fig. 1, as viewed along the hexagonal c_H axis. Oxygen atoms are shown as balls, and hydrogen bonds as connecting sticks. Hydrogen atoms are not shown. The oxygen atoms of type O(2), which lie on three-fold axes, are shown displaced left and right from their actual positions so as to make visible the fact that there are bonded O(2)$\cdots$O(2′) pairs. The actual O(2) positions are directly above and below the centers of symmetry, which are shown as small circles. The oxygen atoms that are not near marked centers of symmetry in Fig. 1 are all of type O(1).

The structure depicted in Fig. 1 is a tetrahedrally linked network of hydrogen bonds in which each water molecule, represented by its oxygen atom, is hydrogen bonded to four others. This feature is present in all of the known ice structures. In ice IV, the bonds form a single network extending throughout the crystal. Ice IV is the densest ice phase in which high density is achieved with such a structure; in ices VI, VII, and VIII there are two separate, interpenetrating but not interconnecting bond networks (the "self-clathrate" feature[15]). Unlike several of the other ice structures,[15,16] the bond network of ice IV has no analog among tetrahedrally linked frameworks in structures of SiO_2 or silicates.

The O(1)-type atoms are bonded together in puckered six-rings of $\bar{3}$ symmetry, five of which are visible in Fig. 1. Similar six-rings occur in ice I and several other ice structures. The extent of puckering, as measured by the departure of individual atoms from the mean plane of the six-ring, is considerably less in ice IV (17 pm) than in ice I (46 pm), and somewhat less than in ice II on average (31, 13 pm for two nonequivalent six-rings). No smaller rings are present, in contrast to ices III, V, and VI, which contain five- and four-rings.[12,15,16]

Though the center of each O(1)-type six-ring (marked by a symmetry center in Fig. 1), along the three-fold axis, runs an H-bond between a pair of O(2)-type atoms that lie symmetrically above and below the ring. This structural motif of eight atoms, an O(1)-type six-ring with an O(2)-type pair bonded through the ring's center, is illustrated in Fig. 2. Two such motif units make up the contents of the rhombohedral unit cell.

TABLE IV. Approximate positions of hydrogen atoms in ice IV.

	Centerline[b]			Refined[c]		
Atom	x	y	z	x	y	z
$\frac{1}{2}$H(3)[a]	0.03	0.03	0.03	0.03	0.03	0.03
$\frac{1}{2}$H(4)	0.15	0.19	0.01	0.14	0.18	0.01
$\frac{1}{2}$H(5)	0.20	0.28	−0.05	0.21	0.33	−0.10
$\frac{1}{2}$H(6)	0.29	0.01	−0.29	0.30	−0.01	−0.28
$\frac{1}{2}$H(7)	0.20	0.12	−0.33	0.22	0.11	−0.34
$\frac{1}{2}$H(8)	0.25	0.47	−0.04	0.28	0.41	−0.02

[a]Position type 4*c*. All others are type 12*f*.

[b]On O$\cdots$O centerlines 98 pm from each oxygen.

[c]After least-squares refinement as described in text. Estimated standard deviation approximately 0.02.

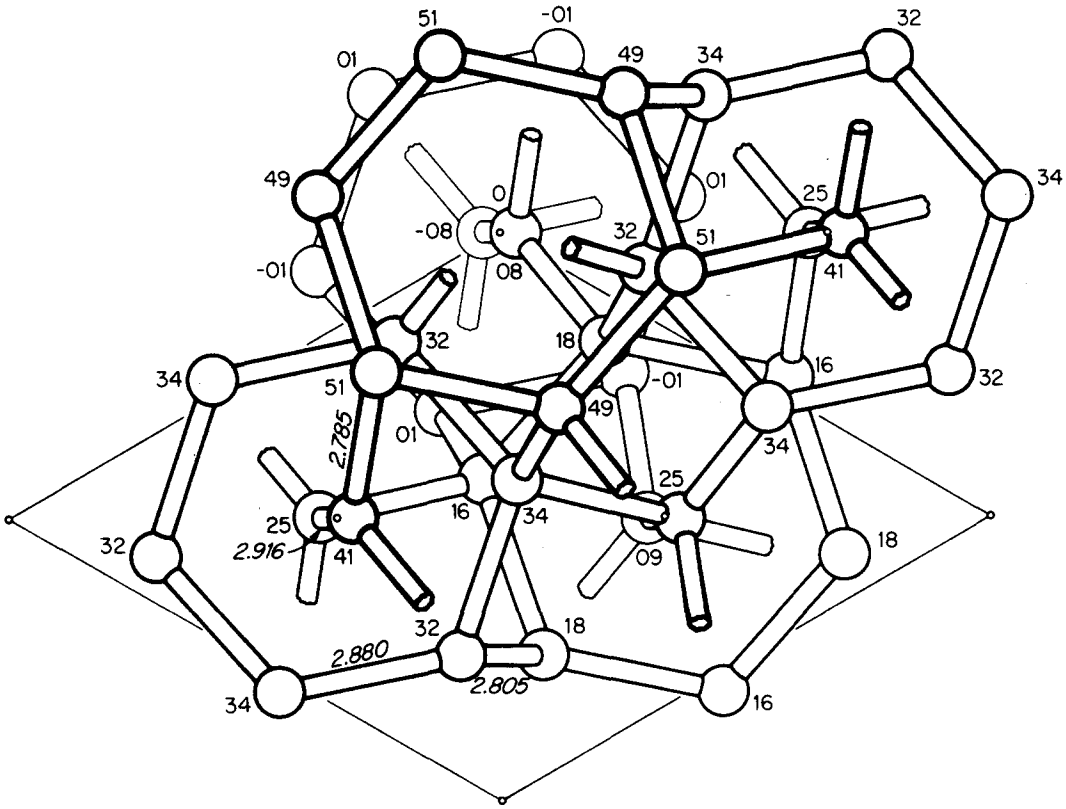

FIG. 1. Structure of ice IV as seen looking along the hexagonal c_H axis (of length 17.05 Å). Oxygen atoms are shown as balls, and hydrogen bonds as connecting sticks. Centers of symmetry are shown as small circles. The hexagonal unit cell is outlined, its edges being the a_H axes, of length 8.74 Å. Origin of coordinates is at the symmetry center in the upper middle. Heights of atoms above projection plane through origin are shown in hundredths of the c_H-axial length. The rhombohedral axis a_1 runs from the origin down and left to the symmetry center near the tip of the arrow marked "2.916," which is at height $c_H/3$; axis a_2 runs from the origin to the symmetry center in the upper right; a_3 runs up and left. Each symmetry center lies on a threefold axis (actually $\bar{3}$ axis) parallel to c_H. The c glide planes (parallel to c_H, follow the traces of the rhombohedral a_R axes. Twofold axes follow the traces of the a_H axes; for example, one at height $c_H/4$ runs straight down from the upper to the lower corner of the hexagonal cell. The atoms that occur in pairs at heights ±08/100 above and below the symmetry centers are of type O(2). They are shown displaced slightly left and right from their exact positions on the threefold axes, so that the bonded O(2) ···O(2′) pairs can be seen. All other atoms are of type O(1). For clarity, not all atoms in a unit cell (either rhombohedral or hexagonal) are plotted. Decimal numbers show H-bond lengths in Å.

A related structural motif occurs in ice V, where a bond between atoms of type O(4) threads through the center of an eight-ring,[7] the ring center being again a center of symmetry. The noteworthy feature of these ring threadings in ice IV and V is that the atoms that bond through the ring center do not bond directly to the ring; they are linked to it only indirectly, through two or more intervening atoms. Thus, in ice IV, the shortest connection from each O(2) atom to its adjacent six-ring is via two intervening O(1)-type atoms (as can be seen in Fig. 2), there being by symmetry three such connections; and in ice V, the shortest connections are again via two intervening atoms, there being two such connections from each O(4) atom to the adjacent eight-ring. In the self-clathrate structures, bonds of one framework thread through rings in the other, and there is no bonding connection at all between the two; in ice VI the smallest rings threaded are eight-rings, while in ices VII and VIII they are six-rings. Ring threading in the sense just considered is not found in ice phases less dense than ice V. Its appearance in ices IV and V seems thus to be a feature transitional to the self-clathrate type of structure found in the densest ice phases.

The way in which the structural motif (six-ring plus O(2)-type bonded pair) is linked outward to others to form a three-dimensional bond framework can be seen in Figs. 1 and 2 and is shown in stereoscopic view in Fig. 3. Every O(1)-type atom in the six-ring bonds laterally outward to an O(2)-type atom of a separate motif unit; reciprocally, each O(2)-type atom links together three six-rings of separate motif units; collectively these linkages form bonded layers, as shown in Fig. 4. Every O(1)-type atom also sends a bond either upward or downward to another O(1)-type atom in a separate six-ring at a height $\pm c_H/6$ above or below the first. These O(1)··· O(1‴)-type bonds, of which the ones labeled "2.805" in Figs. 1 and 2 are examples, are centered on two-fold axes. Together with the O(2)··· O(2′)-type bonds, they link the structural layers (Fig. 4) together in the general direction of the c_H axis.

Although the structure of ice II[17] is based on a bond framework in the same space group ($R\bar{3}c$) as ice IV, there is no intimate relationship between the two struc-

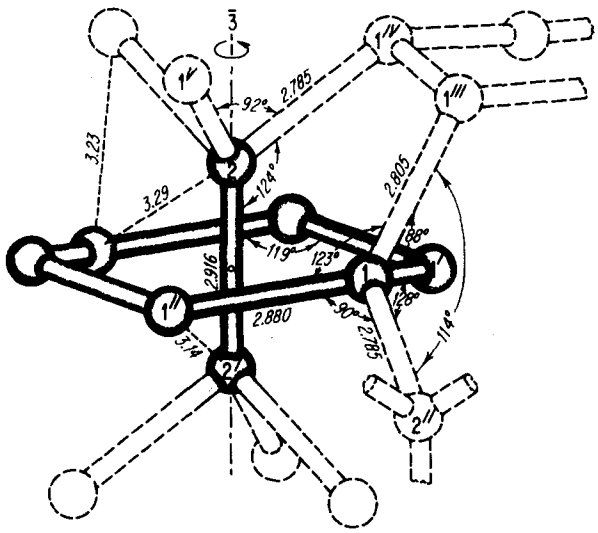

FIG. 2. Structural motif of ice IV, consisting of an O(1)-type six-ring plus an O(2)-type pair bonded through the ring's center. This motif unit is drawn with solid lines and accentuated with shading. Some of its connections to adjacent parts of the structure are shown with dashed lines. The $\bar{3}$ axis along which the O(2) ···O(2′) bond runs is indicated, and the associated inversion center is shown as a small open circle. O(1)-type atoms are labeled 1, 1′, 1″, etc. and O(2)-type 2, 2′, etc. At the upper right is part of a second O(1)-type six-ring, and at the lower right the top of a second O(2)-type bonded pair. H-bond lengths and short non-H-bonded distances, in Angstroms, are marked. H-bond angles (O ···O ···O angles) around O(1) and O(2) are shown. The 119° angle O(1′) ···O(1) ···O(1″) is given for clarity at a symmetry-equivalent position in the six-ring, related to O(1) by the threefold axis.

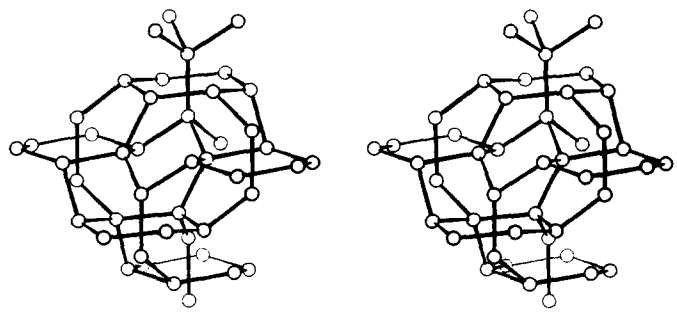

FIG. 3. Stereoscopic view of a portion of the ice IV structure, seen at a high angle to the hexagonal c_H axis, which runs up and down in the diagram and is tilted about 10° out of the plane of the paper. The diagram includes five O(1)-type six-rings and associated O(2)-type pairs bonded through the ring centers along the c_H axis. From the uppermost to the lowermost ring is $c_H/2$, and from the uppermost ring to the ring most in front is a_R.

tures, the only common feature being the presence of puckered six-rings of $\bar{3}$ symmetry. In ice II, these rings are bonded one above the other as in ice I to form hexagonal columns parallel to c_H, which is a bond arrangement very different from that in ice IV, as explained in the next section.

VII. RELATIONSHIP TO ICE Ic STRUCTURE

The structural layers emphasized by the representation in Fig. 4 are topologically identical to the puckered

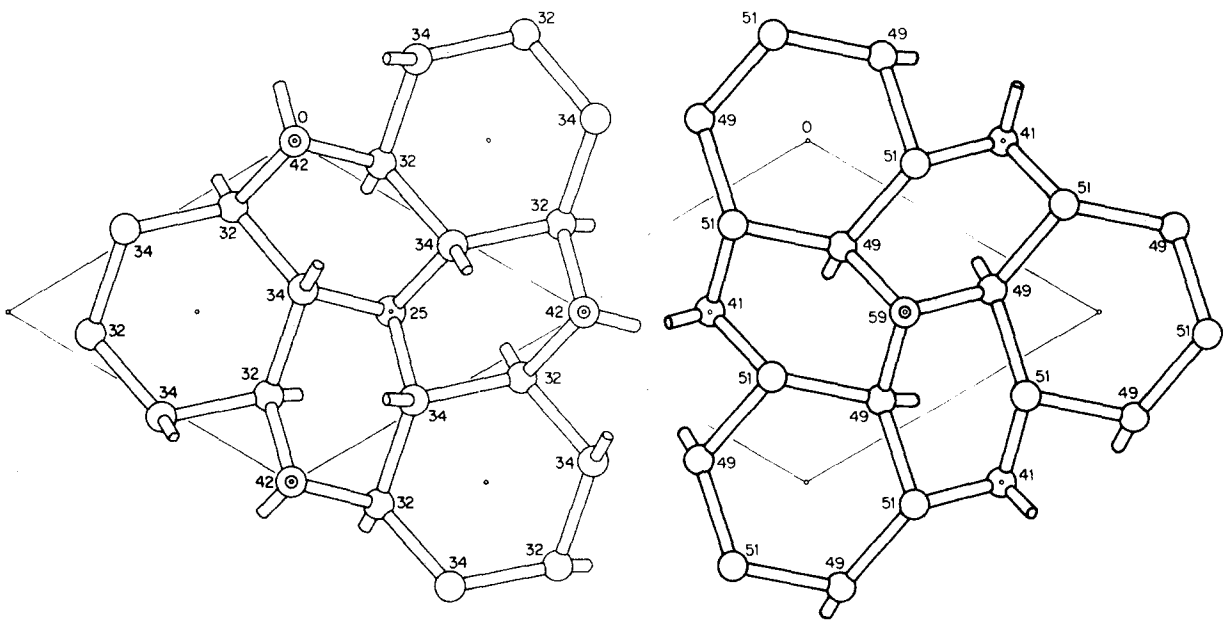

FIG. 4. Parts of the structure of ice IV, isolated so as to emphasize the structural layers in planes perpendicular to the c_H axis. Orientation and conventions are as in Fig. 1, except that the O(2)-type atoms are shown in their actual positions rather than laterally displaced as in Fig. 1. On the left is shown the bonded layer centered at height $c_H/3$, and on the right the layer at $c_H/2$ is shown separately, each layer in relation to the hexagonal unit cell as marked with light lines.

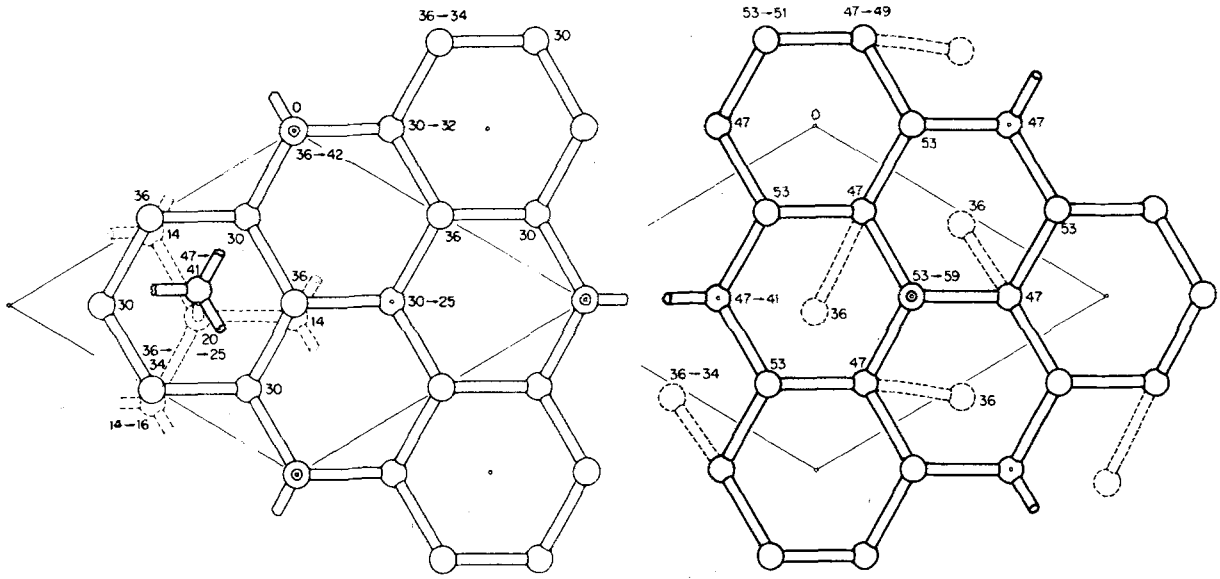

FIG. 5. Bond pattern generated from Fig. 4 by rotating the O(1)-type six-rings ±12° around the c_H axis. Vertical coordinate figures, fragments of additional layers on the left, and dashed bonds on the right are included to correspond with Fig. 7.

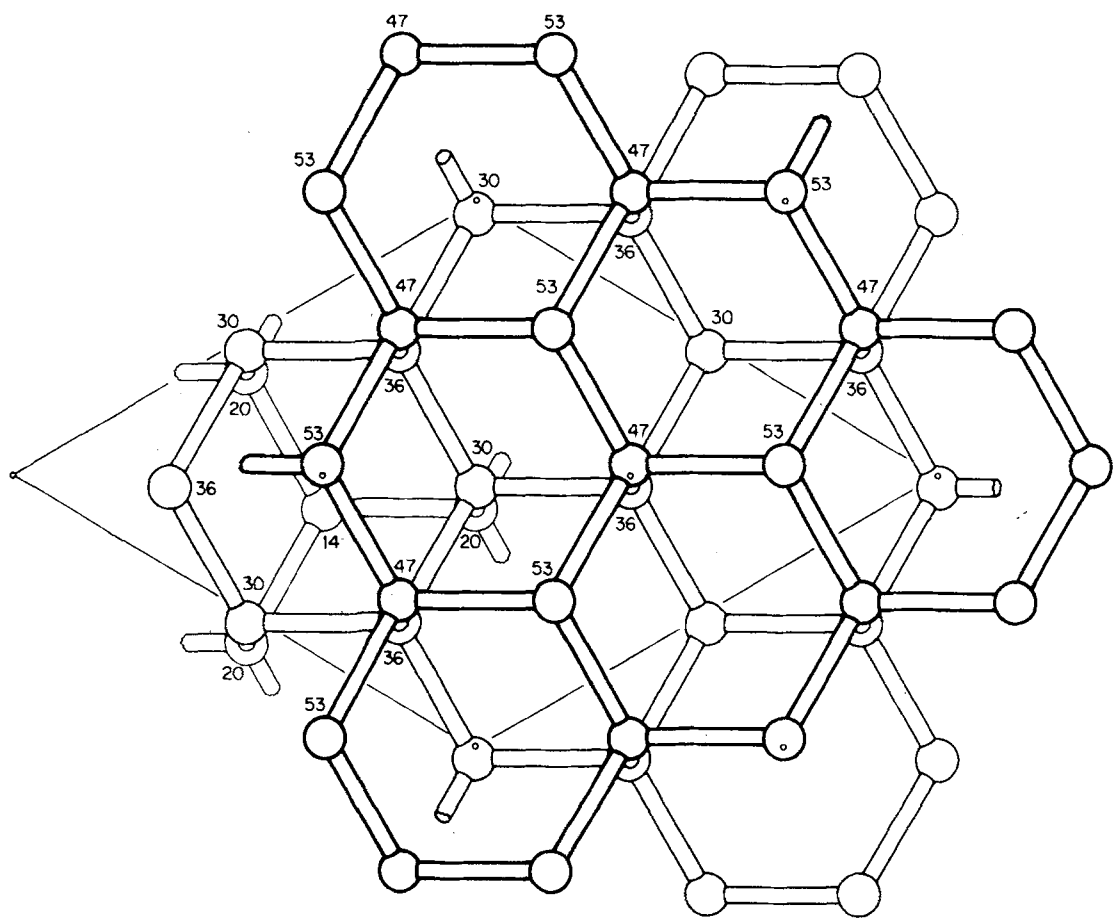

FIG. 6. Structure of ice I_c seen in projection on the (111) plane, which is here represented as the basal plane of an equivalent hexagonal cell whose edges are outlined and whose c_H axis, perpendicular to the drawing, is of length 22 Å. The puckered hexagonal layers parallel to the basal plane are slightly offset laterally so that bonds between the layers, parallel to the c_H axis, are visible.

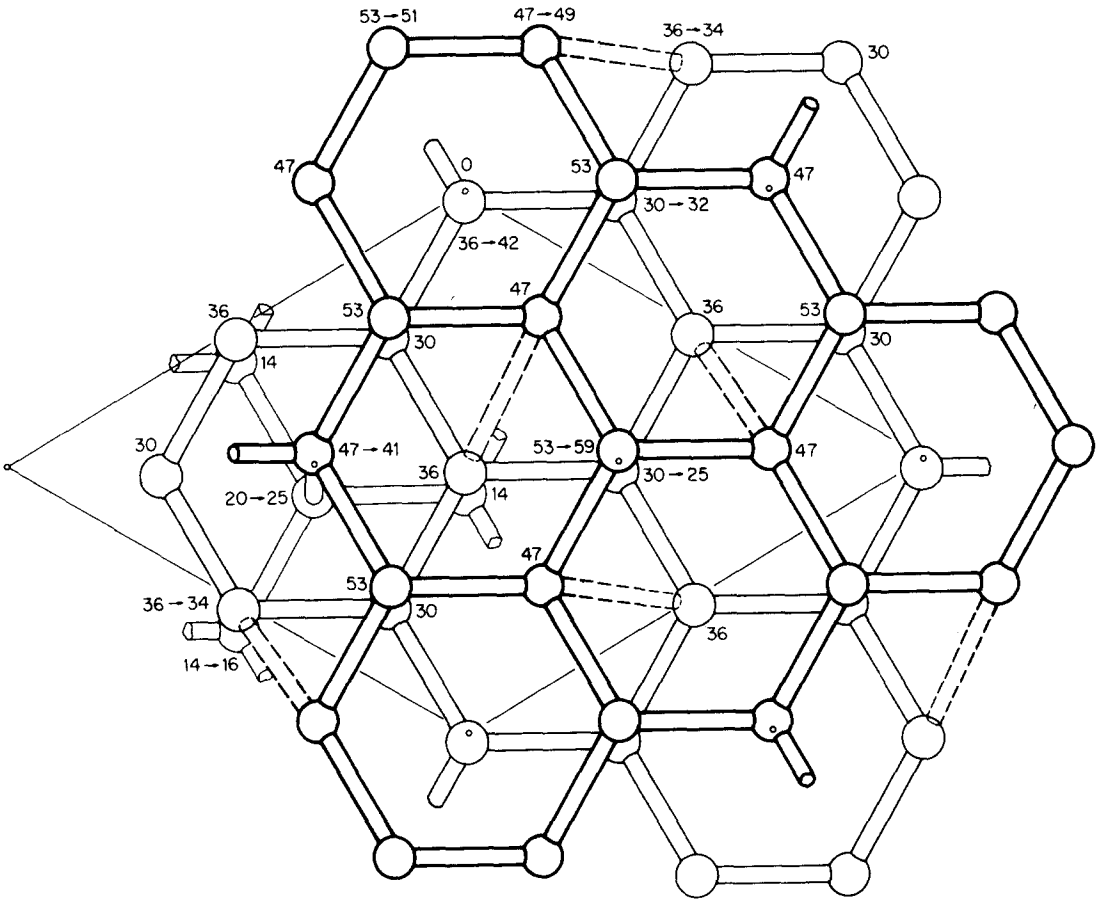

FIG. 7. Arrangement that results from Fig. 6 by cutting all interlayer bonds, reversing the puckering of the layers, and reconnecting nonadjacent layers by c_H-parallel bonds passing through centers of six-rings in the intervening (middle) layer. It represents an assembled view of the components shown in Fig. 5. The changes in height coordinates indicated by the arrows are vertical adjustments that have to take place for the new bonds to form. Dashed lines show additional interlayer bonds that will form in the further adjustment leading to Fig. 8.

hexagonal layers in the structure of Ice I (parallel to the basal plane) and of ice Ic (parallel to {111}). The similarity is accentuated if the O(1)-type six-rings are rotated ±12° around the c_H axis, producing the bond pattern in Fig. 5. We now show that there is a detailed, though circuitous, relationship between the ice IV and ice Ic structures, whose recognition aids geometrical comprehension and brings out a particularly remarkable feature of the ice IV structure.

The relationship is developed by deriving the ice IV structure from ice Ic in the sequence of steps in Figs. 6–8. Figure 6 shows the cubic ice Ic structure in relation to an equivalent hexagonal unit cell, which the cubic geometry permits, the projection plane being the (111) plane of the cubic cell. Parts of three puckered hexagonal layers are shown, centered at heights $c_H/6$, $c_H/3$, and $c_H/2$ in relation to a hexagonal c_H axis that is of length 22 Å in the undistorted ice I_c structure and contracts to 17 Å in going over to the ice IV structure (Figs. 7 and 8). To go from the arrangement in Fig. 6 to that in Fig. 7, all of the bonds parallel to the c_H axis, between the hexagonal layers, are broken and the puckering of all layers is reversed, which is shown in Fig. 7 by the changed assignment of height coordinates (whose numerical values are chosen so that the puckering represented is the same as that in ice Ic when the coordinates refer to a 17 Å c_H axis). After the reversal of puckering, it becomes possible to form a new c_H-parallel bond from the uppermost to the lowermost layer, passing through the center of a puckered six-ring of the intervening middle layer, as shown in the left-hand part of the unit cell in Fig. 7. For this bond to shorten to a length of about 2.9 Å, the two atoms involved have to approach one another by moving farther out of the planes of their respective layers, as shown by the change in height coordinates following the arrows in Fig. 7.

The formation of the bond linking two nonadjacent structural layers and passing through the intervening layer is a remarkable structural feature, not previously described in a layer structure, as far as we are aware; This bond is the O(2)···O(2′)-type bond described in the previous section. Only one such bond is shown in Fig. 7 because of the limited extent of the lowermost layer as drawn, but every O(2)··· O(2′)-type bond in the structure is identical and is formed in the same way.

The final step leading to ice IV, shown in Fig. 8, is to complete the reconnection of the previously separated

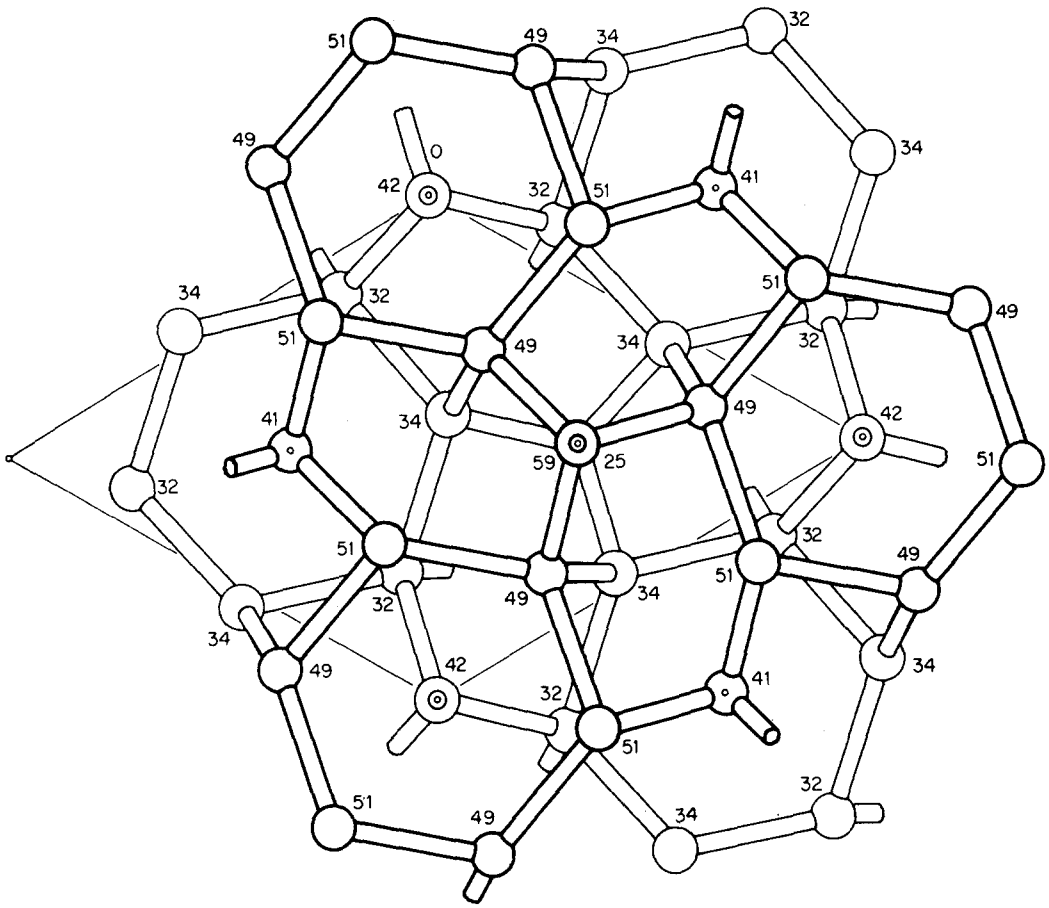

FIG. 8. Structure of ice IV, derived from Fig. 7 by ± rotations of six-rings centered on symmetry centers, resulting in formation of new interlayer H bonds by shortening of the dashed distances in Fig. 7. Notation and conventions are the same as in Fig. 1, except that O(2)-type atoms are shown in their actual, undisplaced positions, and O(2)–O(2′)-type bonds parallel to the c_H axis are shown end-on. The two structural layers shown assembled here are the ones shown separately in Fig. 4. For clarity, the fragment of the lowest layer in Figs. 6 and 7 is omitted here, but part of it is visible in the bottom half of Fig. 1.

layers by forming additional interlayer bonds, shown dashed in Fig. 7. This is accomplished by counterrotation of six-rings in adjacent layers, which shortens the dashed distances to H-bond lengths. The new interlayer bonds are of the type earlier called O(1)··· O(1‴), centered on two-fold axes. The six-rings that rotate are those not constrained by the O(2)··· O(2′)-type interlayer bonds previously formed; after rotation they become identifiable as the O(1)-type six-rings described earlier. The intervening six-rings of the puckered hexagonal layers become markedly elliptical (see Fig. 4).

Because of the rotation of six-rings in opposite directions (+ and −) in alternate layers, the layer stacking sequence of type ABCABC... inherited from the cubic structure of ice Ic becomes modified to $A^+B^-C^+A^-B^+C^-$.... As a result, the c_H axial repeat in the IV involves six layers.

VIII. HYDROGEN BONDING AND MOLECULAR PACKING

Hydrogen bonds in the ice IV structure, as in other ice structures,[6] are recognizable as O··· O distances that group in the range from 275 to about 290 pm and that as a group are distinctly set off from distances longer than about 320 pm. The presence of four such distances in roughly tetrahedral orientation around each oxygen atom, as shown in Figs. 1 and 2, confirms their identification as H-bonded linkages and conforms to the abundantly observed tetrahedral H-bonding character of the water molecule in ice structures and hydrates. H bonding in ice IV is indicated also by spectroscopic evidence.[4]

Detailed characteristics of the H bonds in ice IV at 1 atm pressure are given in Fig. 2 and Tables V and VI. The H-bond lengths, listed as group 1 in Table V and identified in Fig. 2, are noteworthy in the presence of two extraordinarily long bonds, those of lengths 288 and 292 ± 1 pm. These are the longest bonds in any of the ice phases except VII and VIII, which contain bonds of length 295 pm (at 1 atm). Aside from these, the longest bond in any of the other ice phases is one of length 286.7 pm in ice V.[12] The mean bond length for ice IV (weighted by the bond multiplicities listed in Table V) is 283.3 pm; this is the largest of the mean bond lengths in all of the ice phases except VII and VIII.[6]

The probable cause of the long H bonds in ice IV is the presence of short non-H-bonded contacts between the molecules in the structure, at distances short enough

TABLE V. Oxygen–oxygen distances in ice IV, at 1 atm, 110 K.

Distance group[a]	Atom pair[b]	Distance (Å)	σ(Å)[c]	Multiplicity[d]
1	O(1)···O(2″)	2.785	0.005	6
	O(1)···O(1‴)	2.805	0.008	3
	O(1)···O(1′)	2.880	0.007	6
	O(2)···O(2′)	2.916	0.010	1
2	O(1)···(2)	3.14	0.01[e]	6
	O(1′)···O(1′ᵛ)	3.23	0.01	3
	O(1)···O(2′)	3.29	0.01	6
3	O(1)···O(1*)	3.81	0.01	3
	O(1′)···O(1‴)	3.95	0.01	3
	O(1″)···O(2″)	4.01	0.01	6
	O(1)···O(1*)	4.08	0.01	3

[a]Group 1 represent hydrogen bonds, group 2 are short non-H-bonded distances, and group 3 are all longer distances up to 4.6 Å.

[b]Atoms are identified in Fig. 2. Symmetry-equivalent atoms are designated with primes. A superscript * indicates other atoms, not labeled in Fig. 2.

[c]Estimated standard deviation calculated by propagation-of-error methods from the standard deviations of the hexagonal coordinates estimated in the least-squares refinement (Ref. 14), with account taken of the particular combinations of coordinates that enter into the individual bond distances.

[d]Number of distances per group of eight oxygen atoms.

[e]Estimated upper bound.

that significant intermolecular repulsion operates. The particularly short nonbonded oxygen–oxygen distances are listed in group 2 of Table V. The O(1)–O(2) distance of 314 pm is distinctly shorter than the shortest nonbonded oxygen–oxygen distances in other ice phases (again excepting VII and VIII), namely, 324 pm in ice II and 328 pm in ice V. The remaining group-2 distances in Table V are comparable to these shortest distances in other phases. The bipyramidal geometry of the short nonbonded contacts in the eight-molecule motif unit in Fig. 2 is such that if intermolecular repulsion operates at distances of 314 and 329 pm, it will force a stretching of the O(2)···O(2′) bond, and also of the O(1)···O(1′)-type bonds in the six-ring. This explains qualitatively the observed lengthening of these bonds.

The magnitude of the bond stretching can be examined quantitatively with use of the overlap energy function derived from experimental data on ice VII.[1] If the eight-molecule motif is treated as an isolated mechanical unit, if the bond-stretching energy function derived for ice I[18] is used, and if results are calculated on the basis of an assumed van der Waals interaction constant[18] $c = 11.7$ kJ mole^{-1}, then for the observed nonbonded contact distances of 314 and 329 pm the predicted lengths of the O(2)···O(2′) and O(1)···O(1′) bonds are 286 and 279.5 pm, which fall considerably short of the observed values 292 and 288 pm. The discrepancy may have several contributory factors: (1) bond bending may increase the unstretched equilibrium bond length and may weaken the bond-stretching force constant; (2) the overlap potential function, derived and tested for ice VII over the nonbonded O···O distance range 286 to 295 pm,[18] may not extrapolate accurately enough to distances in the range 310–330 pm; (3) other forces, from outside the eight-molecule unit, may contribute significantly to the bond lengths. A similar situation was noted in the case of bond stretching in ice II.[18]

As has been recognized in the other dense ice phases,[6] the accommodation of increasing numbers of nonbonded molecular neighbors at relatively short distances is the geometrical feature by which increased molecular packing density is achieved in these tetrahedrally H-bonded structures. Increased packing density leads to progressive lengthening of the H bonds because of repulsion between the nonbonded near neighbors and because of bond bending. Ice IV conforms to this pattern and, next to ice VII/VIII, represents an extreme in terms of lengthening of the mean bond distance (discussed above) and in terms of the number of nonbonded neighbors at distances less than 330 pm. The water molecules in ice VII/VIII have four nonbonded neighbors in the distance range 280–315 pm. In ice IV, the water molecules have, on average, 3.75 neighbors in the distance range 310–330 pm, whereas in ice II they have only one such and in the other ices fewer than one.[6(a)] Distances in the range 330–350 pm only partly redress this difference, except for ice VI, in which each water molecule has, on average, 8.25 neighbors at about 350 pm. At this distance, the intermolecular repulsion has evidently decreased enough that, in spite of their large number, the effect of these contacts in stretching the bonds (average length 281 pm in ice VI) is less than that of the smaller number of shorter contacts in ice IV.

With regard to hydrogen-bond bending, ice IV is also intermediate between ice VII/VIII and the other dense ice structures. The O···O···O bond angles, which provide a basic constraint on H-bond bending, are listed for ice IV in Table VI and illustrated in Fig. 2. A substantial departure from ideal tetrahedral coordination geometry is seen in the deviation of the bond angles from the tetrahedral value 109.5°. While there are no angles near 109.5° (or near 104.5°, the H-O-H angle of the free water molecule), there are also no extreme deviations, the largest being for the angles 88° and 128°. An overall measure of bond bending in ice structures is $\langle(\delta\theta)^2\rangle^{1/2}$, the rms deviation of the O···O···O angles θ

TABLE VI. Coordination angles for H bonding in ice IV.

Bond angle at	Oxygen group	O···O···O angle (deg)
O(1)[a]	O(1′)···O(1)···(1″)[b]	118.7
O(1)	O(1′)···O(1)···O(1‴)	87.7
O(1)	O(1″)···O(1)···O(1‴)	122.7
O(1)	O(1′)···O(1)···O(2″)	127.8
O(1)	O(1″)···O(1)···O(2″)	90.1
O(1)	O(1‴)···O(1)···O(2″)	113.5
O(2)	O(1′ᵛ)···O(2)···O(1ᵛ)	91.8
O(2)	O(1′ᵛ)···O(2)···O(2′)	124.0

[a]Individual oxygen atoms are identified in Fig. 2. Symmetry-equivalent atoms are designated with primes.

[b]In Fig. 2, this angle, the intra-six-ring bond angle (119°), is shown in a position symmetry-equivalent to the O(1′) – O(1) – O(1″) angle, which is hidden in the drawing.

TABLE VII. Bond bending in ice structures as measured by the mean square deviation $\langle(\Delta\theta)^2\rangle$ of O···O···O bond angles from 109.5°. The densities ρ are at 1 atm, 110 K.

Ice	ρ ($g\,cm^{-3}$)	$\langle(\delta\theta)^2\rangle^{1/2}$ (deg)
I	0.94	0
III	1.16	16.4
II	1.18	17.0
V	1.23	18.4
VI	1.31	23.0
IV	1.27	15.7
VII/VIII	1.50	0

from 109.5°. As shown in Table VII, its value for ice IV is lower than for any of the other dense ice structures except ice VII. Table VII shows that for the other ice structures except VII/VIII, $\langle(\delta\theta)^2\rangle^{1/2}$ increases progressively with packing density. It is thus remarkable that while ice IV is 10% denser than ice III, its average bond bending (as measured by $\langle(\delta\theta)^2\rangle^{1/2}$) is actually somewhat lower.

IX. PROTON DISORDER

Order/disorder in the water-molecule orientations, often called proton order/disorder, plays a widespread and important role in the ice phases.[6,19] It is made possible by the asymmetric character of the hydrogen bond for bond lengths of order 250 pm and larger, the proton in such a bond having two alternative sites located about 100 pm from each end of the O··· O linkage. On the basis of entropy estimates, ice IV is proton-disordered under the conditions of its formation at high pressure.[17,20] As observed at 110 K in the present work, ice IV is at least partly proton-disordered, and probably is completely proton-disordered. The evidence for this is as follows.

In the ice IV structure, the center of symmetry at the center of the O(2)··· O(2′) bond and the two-fold axis passing through the center of the O(1)··· O(1‴) bond constrain these bonds to be fully proton-disordered (occupancy probabilities $P_i=\frac{1}{2}$ for the proton sites near both ends of the bonds). The constraint on the O(2)··· O(2′) bond, combined with the sum constraint on the P_i's around O(2) and the symmetry constraint by the threefold axis through O(2), requires $P_i=\frac{1}{2}$ for the proton site adjacent to O(2) in the O(2)··· O(1′ᵛ) bond, and therefore requires full proton disorder for this bond also. These symmetry constraints are required by the space group $R\bar{3}c$, which is unequivocally indicated by the x-ray diffraction data. Any relaxing of the symmetry constraints would necessitate a departure from this space group, which would in turn necessitate giving up at least two of the three c glide planes. Experience with ices II, V, and VI shows that whenever such a symmetry element is given up in the process of proton ordering, the symmetry violation has always proved to be detectable with x rays, even if only weakly. The lack of detectable violation of the c glide planes in ice IV therefore argues strongly for the validity of the symmetry constraints requiring proton disorder.

Only the P_i's in the bonds of type O(1)··· O(1′), forming the six-ring, are not constrained by symmetry to be proton disordered. Because of the $\bar{3}$ symmetry of the six-ring and the sum constraint on the P_i's in each bond, a single independent P_i suffices to describe the state of proton order/disorder in the six-ring. We take it to be P_6, the P_i at site H(6) (Table IV).

An indication as to the value of P_6 was obtained from the x-ray data as follows. After refinement of the oxygen coordinates and introduction of protons with $P_i=\frac{1}{2}$ at all of the centerline sites, a refinement of P_6 was carried out, starting from the value $P_6=0.5$, keeping $P_7=1-P_6$, and holding all positional and thermal parameters fixed. The refinement gave $P_6=0.46\pm0.07$. A second refinement, starting from $P_6=1.0$, converged to the same result. Although the constraint on P_6 provided by the structure factors from x-ray diffraction is necessarily weak, these results imply that the six-ring is probably proton disordered.

If ice IV is fully proton disordered, as the above reasoning (and also spectroscopic evidence[4]) indicates, then it is the only ice phase other than ice I and Ic to remain fully, or even largely, proton disordered on quenching to 77 K. This noteworthy attribute may be due at least in part to the lack in the ice IV structure of any O··· O··· O bond angles very near to 104.5°, which would be especially favorable energetically for H-O-H occupancy, or to the lack of any angles differing extremely from 104.5°, which would be particularly unfavorable.

X. METASTABILITY

The structural basis for the metastable occurrence of ice IV consists of (1) the molecular interaction energetics and packing by means of which ice IV achieves a free energy only slightly higher than ice V and (2) the structural controls on crystal nucleation that allow ice IV to crystallize more readily than the stable phase.

The small free energy difference[21] of about 0.10 kJ mol^{-1} from ice V to ice IV near 5 kb is achieved by offsetting a higher internal energy for ice IV with stabilization due to its higher density. The ΔE from ice V to ice IV is 0.27 ± 0.05 kJ mol^{-1} as estimated from ΔG and the $P\Delta V$ and $T\Delta S$ stabilization contributions,[21] or 0.21 kJ mol^{-1} as estimated[22] independently from Engelhardt and Whalley's[3] observation that $\Delta H=0$ for the ice IV → ice V transition at 4.6 kb.

A structural basis for the experimentally estimated ΔE is provided by the increased number of nonbonded near neighbors in ice IV at distances where overlap dominates van der Waals energy, and by the related increase in H-bond-stretching energy. A quantitative evaluation, based on the bond-stretching, overlap, and van der Waals potentials applicable to ice VII,[18] suggests that these effects are more than sufficient to account for the ΔE. The increase in bond-stretching energy, calculated from the observed H-bond lengths in

TABLE VIII. Dimensional correspondences between lattice planes in ice IV and TCPA. Dimensions are given for pairs of perpendicular lattice vectors in each lattice plane.

	Ice IV		TCPA		
Plane no.	Vector	Length (pm)	Vector	Length (pm)	Mismatch (%)
1	$2a_H$	1748	a	1810	3.5
	c_H	1705	3b	1749	2.5
2	$a_{R1}+a_{R2}$	1244	c	1238	0.5
	$2a_H$	1748	3b	1749	0.05

the ice IV and ice V structures, is 0.48 kJ mol^{-1}. Since most of the overlap and van der Waals energy is associated with the shortest nonbonded distances, we consider the distances in group 2 of Table V and make a comparison between these and an equal number of nonbonded distances in ice V, starting from the shortest and working outward until reaching the same total number of distances (3.75 around each water molecule, on average). If the energy contributions associated with these distances are calculated on the basis of a van der Waals interaction constant $c = 11.7$ kJ mol^{-1} and corresponding overlap interaction constant[18] $b = 16.7$ kJ mol^{-1}, the ΔE contribution for ice IV relative to ice V is 0.73 kJ mol^{-1}. The total calculated ΔE contribution, 1.21 kJ mol^{-1}, is much larger than the ΔE estimated experimentally. This indicates that if the formulation of potential energy as a function of interatomic distance[18] is even roughly correct, there must be major additional sources of intermolecular interaction which to a large extent offset the calculated increase. A contribution of this type comes from H-bond bending, because the extent of bond bending is less in ice IV than in ice V (Sec. VIII). The appropriate bond-bending force constant probably lies between a value 2.5 J mol^{-1} deg^{-2}, based on the observed dependence[23] of internal energy on $\langle(\delta\theta)^2\rangle$ and a value 21.7 J mol^{-1} deg^{-2}, based on molecular libration frequencies and on the elastic shear modulus of ice *I*.[23] The corresponding range of values for the ΔE contribution from bond bending, based on $\langle(\delta\theta)^2\rangle$ values from Table VII, is -0.23 to -2.0 kJ mol^{-1}. Within the wide range of uncertainty here, the calculated ΔE contributions can account for the experimentally estimated ΔE, but because this has to be achieved by the near cancellation of large contributions, its structural basis cannot yet be considered well evaluated quantitatively.

In view of the complexity of the heterogeneous nucleation phenomenon for ice,[24] a simple structural explanation for the reduced barrier to nucleation of ice IV as compared to ice V cannot be expected.[3] If, as has been argued,[25] heterogeneous nucleation is accomplished by monolayers of water molecules adsorbed on solid surfaces, one is tempted to suggest that, because of the structural relation of ice IV to ice I, the presence of adsorbed ice-I-type hexagonal molecular sheets inherited from sample preparation at low pressure may provide a nucleation advantage to ice IV. The structural role of TCPA in nucleating ice IV cannot be based on a simple crystallographic relationship, because the unit cell of TCPA[26] is entirely different in dimensions and symmetry from that of ice IV. However, we find fair to good lattice-dimensional correspondence between ice IV and TCPA for two pairs of crystallographic planes, as shown in Table VIII. Because lattice-dimensional match has been shown to play a role in the nucleation of ice I,[24] it is possible that the relationships shown in Table VIII, or other such relationships not yet discovered, are of significance in the nucleation of ice IV by TCPA.

ACKNOWLEDGMENTS

We thank L. D. Calvert and E. Whalley for making available the experimental facilities at the laboratories of the Canadian National Research Council, Ottawa. R. E. Marsh and Jean Stroll-Westphal helped materially in the crystallographic calculations, and Luise Engelhardt helped in preparation of the manuscript. Peter Pauling prepared Fig. 3.

[1] P. W. Bridgman, Proc. Am. Acad. Arts Sci. **47**, 441 (1912); J. Chem. Phys. **3**, 597 (1935).
[2] L. F. Evans, J. Appl. Phys. **38**, 4930 (1967); K. Nishibata, Jpn. J. Appl. Phys. **11**, 1701 (1972).
[3] H. Engelhardt and E. Whalley, J. Chem. Phys. **56**, 2678 (1972).
[4] H. Engelhardt and E. Whalley, J. Chem. Phys. **71**, 4050 (1979).
[5] A brief preliminary account was published in J. Glaciol. **21**, 51 (1978).
[6] (a) B. Kamb, in *Structural Chemistry and Molecular Biology*, edited by A. Rich and N. Davidson (Freeman, San Francisco, 1968), p. 507; (b) B. Kamb, in *Physics and Chemistry of Ice*, edited by E. Whalley, S. J. Jones, and L. W. Gold (R. Soc. of Canada, Ottawa, 1973), p. 28.
[7] E. Whalley, in *The Hydrogen Bond, Recent Developments in Theory and Experiments*, edited by P. Schuster, G. Zundel, and C. Sandorfy (North Holland, Amsterdam, 1976), Vol. III, p. 1425.
[8] The equipment and facilities for the x-ray experimental work were those of the N.R.C. Chemistry Department, Ottawa, kindly made available by L. D. Calvert.
[9] h, k, 0; h, $h+n$, $l(n=0,1,2)$; $h+l+n$, $-h+l$, $l(n=0,1,2,3,4)$.
[10] J. Waser, Rev. Sci. Instrum. **22**, 563 (1951); R. D. Burbank, *ibid.* **23**, 321 (1952).
[11] (a) A. D. Rae, Acta Crystallogr. **19**, 683 (1965); (b) D. J. Duchamp and R. E. Marsh, *ibid.* B **25**, 6 (1969).
[12] B. Kamb, A. Prakash, and C. Knobler, Acta Crystallogr. **22**, 706 (1967), Table II.
[13] For oxygen: in *International Tables for X-ray Crystallography*, edited by C. H. MacGillavry and R. D. Rieck (Kynoch, Birmingham, 1968), Vol. III, p. 202. For hydrogen: R. F. Stewart, E. R. Davidson, W. T. Simpson, J. Chem. Phys. **42**, 3175 (1965).
[14] Crystallographic calculations were carried out with the CRYSIS and CRYM systems (Caltech IBM 370/3032 computer), in which the rhombohedral structure is handled using the equivalent hexagonal cell. Final results were transformed to rhombohedral coordinates for presentation in Tables I–IV.
[15] B. Kamb, Science **150**, 205 (1965).
[16] B. Kamb, Science **148**, 232 (1965).
[17] B. Kamb, Acta Crystallogr. **17**, 1447 (1964); B. Kamb, W. C. Hamilton, and S. J. LaPlaca, J. Chem. Phys. **55**, 1934 (1971).
[18] B. Kamb, J. Chem. Phys. **43**, 3917 (1965).

[19]L. Pauling, J. Am. Chem. Soc. **57**, 2680 (1935).
[20]A. J. Brown and E. Whalley, J. Chem. Phys. **45**, 4360 (1966).
[21]The ΔG value of 0.10 kJ mol^{-1} at 5.3 kb and about $-15\,°C$, near melting, is estimated from the difference $\Delta T_m = 5.0$ K between the melting points of ice IV and ice V[3] and from the fusion entropy $\Delta S_m \cong 19\ J\,K^{-1}\,mol^{-1}$ determined from the slope dT_m/dP of the melting curve and the volume change on melting.[1] The $P\Delta V$ stabilization of ice IV relative to ice V at 5.3 kb is 0.24 kJ mol^{-1}, as calculated on the basis of the densities 1.320 and 1.277 $g\,cm^3$ estimated at this pressure for ice IV (Sec. III) and ice V (Ref. 12), from crystallographic data. The somewhat uncertain, but small, ΔS between ice IV and V (0.08 $J\,K^{-1}\,mol^{-1}$ based on data of Bridgman[1] for D_2O ice IV, 0.42 $J\,K^{-1}\,mol^{-1}$ based on data of Engelhardt and Whalley[3] for H_2O ice IV) corresponds to a stabilization of 0.07 ± 0.05 kJ mol^{-1} in favor of ice V at $-7\,°C$, 5 kb.
[22]The ΔE estimate obtained by Engelhardt and Whalley (Ref. 3) is here re-evaluated with use of the densities stated in footnote 21.
[23]Reference 6(a), p. 514 and Fig. 7.
[24]P. V. Hobbs, *Ice Physics* (Clarendon, Oxford, 1974), pp. 493–523.
[25]L. F. Evans, Nature London **213**, 384 (1967); G. R. Edwards and L. F. Evans, J. Atmos. Sci. **28**, 1443 (1971).
[26]W. C. McCrone, Anal. Chem. **23**, 1339 (1951).